

# Finite Elements Analysis of CFRP Specimens with Included Cracks

PAUL DORU BARSANESCU<sup>1</sup>, PETRU CARLESCU<sup>2</sup>, VIOREL GOANTA<sup>1\*</sup>, IONUT DUMITRASCU<sup>1</sup>

<sup>1</sup> Gheorghe Asachi Technical University of Iasi, Faculty of Mechanical Engineering, 61-63 Dimitrie Mangeron Blvd., 00050, Iasi, Romania

<sup>2</sup> University of Agricultural Sciences and Veterinary Medicine Iasi, 3 Mihail Sadoveanu Alley, 700490, Iasi, Romania

*The paper presents the development of a cross-ply composite material reinforced with carbon fibers and epoxy matrix (CFRP). Specimens cut from composite plate have been tested in tensile, using a testing machine with hydraulic grips, assisted by full-field strain measurements equipment. Using tensile tests and ultrasounds technique, were determined the nine elastic characteristics of the orthotropic material. During tensile test, at a certain level of stress, inside the specimen, small cracks appear. These cracks become more numerous and larger with increasing of stress. A portion of a specimen without cracks and with cracks respectively, subjected to tensile, were simulated by Finite Elements Analysis (FEA). For this analysis, the composite material was considered homogeneous and orthotropic. The simulation of cracks presented inside the specimens at different stress levels has been realized using X-ray pictures. Based on the FEA determinations, the stress state in the vicinity of the cracks was determined.*

**Keywords:** carbon fibers, laminate, matrix cracking, finite element analysis (FEA)

CFRP composites are high-performance materials. They were originally used in space industry, aircraft construction and defense. Because of their special properties, these materials are now more and more used in automotive industries or civilian applications.

The damage mechanism in composite materials is much more complex compared with that in conventional materials such as steel or aluminum and are governed by fiber type, matrix type, architecture and loading conditions. The microstructural mechanisms of damage accumulation in CFRP include: matrix cracking, fiber/matrix debonding, transverse-ply cracking, delamination and fiber breakage [1-5].

For most of the composites loaded in tensile the initial cracking relates to transverse cracks in fiber bundles, which are not parallel to the loading direction (0°). In general, in the 90° ply of cross-ply laminates, the matrix cracks are generated at a lower applied strain under a tensile load [4, 6, 7]. Those transverse cracks cause interlaminar delamination and fiber breakage in the 0° ply at a higher applied strain. Using the pictures taken by X-ray technique was seen as at a certain level of stress, small cracks appear in samples subjected to tensile [4, 7]. Micro cracks in CFRP are hard to see by X-ray inspection, but their presence can significantly affect the composite properties. These cracks become more numerous and larger with increasing of load [7, 8]. We can say that the stages of transverse cracking are:

- fiber-matrix debonding and matrix micro-cracking;
- growing of matrix cracks into transverse ply cracks which initiate delamination.

Often the cracks initiate in the vicinity of free edges, where residual stresses can be very high. Usually, higher residual stresses result in a higher microcrack density. The perpendicular cracks are most often observed. Typically they grow from the edges to the center of the sample, where possibly can be joined [7, 9].

The transverse cracks affect in many ways the composite properties [9, 10]:

- decreasing of strength, stiffness, elastic module, Poisson's ratio, interlaminar fracture toughness and endurance with increasing microcrack density;

- increasing creep deformations;
- lower resistance for corrosive liquids;
- increased capacity to absorb moisture;
- decreases the transverse electrical conductivity of CFRP.

Based on FEA, the stress state in the cracked composite was determined using X-Rays, after the composite was loaded at different stages of stresses. Can be seen the changing of state of stress in the specimen depending on the nominal tensile stress level, the number and size of cracks, almost the breaking of the specimen.

## Composite plates manufacture

### Lamina

Unidirectional carbon fiber/Epoxy prepreg, type Q-1112 1480, manufactured by TohoTenax, with thickness 0.15 mm was used to manufacture CFRP plates. Reinforcement is done by high strength (HS) Carbon fiber STS40 24K type. Some characteristics of unidirectional reinforced lamina are: matrix type - epoxy, fiber Young modulus 242 [GPa], fiber strength 4240 [GPa], elongation 1.75 [%], fiber diameter 7 [μm], the areal density of the prepreg is 202 [g/m<sup>2</sup>].

### Manufacturing technology

To produce a composite plates with dimensions of 300×300 mm, nine prepreg layers as above were stacked one on top of the other in the storage sequence [(0/90°)<sub>s</sub>]. Then, the prepreg layers were cured at 90°C for 60 min followed by a post curing step at 130°C for 90 min. The laminates were produced in an autoclave at vacuum of -0.697 to -0.700 [MPa].

Plates so made have had a thickness around 1.30 mm, fiber volume fraction 71% and density 1.44 g/cm<sup>3</sup>. The fiber volume fraction of composites was determined using matrix digestion method with sulfuric acid and hydrogen peroxide, described in standard ASTM D 3171 [11].

A significant number of specimens cut from different parts of CFRP plates were examined under optical microscope. No micro defects (voids, micro cracks etc.) were found by this inspection. A good impregnation of prepreps where observed.

\* email: paulbarsanescu@yahoo.com

Material	E <sub>1</sub>	E <sub>2</sub>	E <sub>3</sub>	G <sub>12</sub>	G <sub>13</sub>	G <sub>23</sub>	ν <sub>12</sub>	ν <sub>13</sub>	ν <sub>23</sub>
	[GPa]								
Cross-ply Epoxy	86	81	2.53	4.36	2.94	0.88	0.15	0.30	0.44

**Table 1**  
ELASTIC CHARACTERISTICS  
OF THE CROSS PLY CFRP  
COMPOSITE (71% C)

### Elastic characteristics of the composite

The elasticity of an orthotropic material is defined by nine "engineering characteristics":

- Young's modul  $\nu_{12}$ ,  $\nu_{13}$ ,  $\nu_{23}$ ;
- Shear modules  $G_{12}$ ,  $G_{13}$ ,  $G_{23}$ .

Tensile tests were made to determine the ultimate stress, elastic characteristics  $E_1$  and  $\nu_{12}$ . Four samples with dimensions of 260×25 mm were cut of CFRP plate, oriented in the fiber direction, using a diamond saw cutting machine. Fiberglass end-tabs with dimensions of 40×25 mm have been glued onto the tensile samples, using two-component epoxy glue (Araldite 2011, Huntsmann). The glue was cured at 100°C for one hour. The sample length between the fiberglass end tab was around 177 mm.

Tensile tests were performed on a testing machine Instron 4505 with a load cell of 100 kN and hydraulic grips, according to ASTM D3039 [12]. The test speed was 1 mm/min. The tests were assisted by full-field strain measurements equipment (also called strain mapping) LIMESS Messtechnik, which involves comparing images recorded in the same region of the specimen, initially and throughout the test. For this purpose, the specimen surface is painted with two contrasting colors (white background with black spots). During the test, a camera is focused on the central area of the specimen. At set intervals (1 s in our experiment), a digital image of the sample surface is taken and then it is stored on computer. The monitoring the displacement and deformation of the black spots, allows the Limess Vic2D software to quantify the plane deformation of the sample. The strain mapping techniques can be used as a 2D optical extensometer. The strains  $\epsilon_1$  and  $\epsilon_2$  in longitudinal and transversal direction respectively are calculated with an accuracy of about 0.01%.

The stress-strain diagrams were drawn using the connection between Instron testing machine and optical equipment Limess. The Young's modulus  $E_1$  was determined as the slope of a stress-strain curve in the linear part, from 0.1 and 0.3% of strain. The Poisson's ratio  $\nu_{12}$  was calculated by the longitudinal  $\epsilon_1$  and transverse  $\epsilon_2$  strains, using data from the Limess system. The average ultimate stress for the four samples is 1330MPa.

The elastic characteristics of orthotropic material were determined using tensile tests and ultrasounds technique [13-17]. In order to measure the wave velocities, a system using two ultrasound transducers type MB4Y - General Electric USA used in transmission technique, a Pulser Receiver 5077PR-Panametrics USA and digital oscilloscope Le Croy Wave Runner 64Xi that measures the time intervals has been used. Knowing these speeds the elastic characteristics  $E$ ,  $\nu$  and  $G$  can be calculated [17]. The elastic characteristics of the orthotropic composite are presented in table 1.

### Finite Elements Analysis

During tensile test, at a certain level of stress, in sample small cracks appear. These cracks become more numerous and larger with increasing of stress. In X-ray pictures one can clearly see cracks in the specimen at different stress levels [7]. For a cross-ply composite, first cracks appear in plies oriented at 90° and do not propagate through the plies oriented at 0°. Thus, these cracks appear inside the material and are closed.

A portion of a specimen without cracks and with cracks respectively, subjected to tensile, were simulated by Finite Elements Analysis (FEA), using Abaqus V 6.12 software [18]. The dimensions of sample included in the modeling and simulation were: length by Ox axis - 100 mm, width by Oy axis - 25 mm and thickness by Oz axis - 1.3 mm. The calculation process for all specimens were performed with TYAN graphics station, having two processors Intel Xeon Six Core 3.33 GHz, two boards Tesla Fermi C2050 and 32GB DDR3 RAM memory.

For this analysis, the composite material was considered homogeneous and orthotropic, with the elastic characteristics shown in table 1. The good simulation of cracks presented in specimens of similar material has been realized using X-ray pictures [7] and Image-Pro Plus software for lengths measuring (fig. 1).

In order, to compare the results obtained with FEA with some known from the literature, and which allow then to obtain the new results, the simulation was made for the following situations:

- sample made of homogeneous and orthotropic material, without cracks ( $\sigma = 300$  MPa);
- sample made of homogeneous and isotropic material, with pierced cracks ( $\sigma = 300$  MPa);
- sample made of homogeneous and orthotropic material, with pierced cracks ( $\sigma = 300$  MPa);
- sample made of homogeneous and orthotropic material, with inside cracks ( $\sigma = 300$  MPa,  $\sigma = 625$  MPa,  $\sigma = 725$  MPa ).

#### *Sample made of homogeneous and orthotropic material, without cracks ( $\sigma = 300$ MPa)*

In the first step of the analysis was simulate a specimen without cracks, made of homogeneous and orthotropic material, embedded at one end and subjected to tensile with uniformly loading distributed throughout the all section. The specimen mesh without cracks was performed using 170,424 finite elements type brick (structured).

#### *Sample made of homogeneous and isotropic material, with pierced cracks ( $\sigma = 300$ MPa)*

From literature are not known analytical, numerical and experimental results for the stress tension on the tip crack situated inside (in the middle) of the orthotropic material. For check this results, was first studied a homogeneous and isotropic material, where the crack is pierced (i.e. the entire thickness of the specimen), known case from Fracture Mechanics [20, 21]. Since, this modeling is done only for the purpose of verification, the elastic characteristics of the isotropic material were taken  $E = 200$  GPa and  $\nu = 0.3$ .

In specimen were introduced three cracks, as shown in figure 1a, with the dimensions:  $L \times l \times h = 2.5 \times 1.3 \times 0.1$  mm. Then the specimen was simulated to tensile loading up to  $\sigma = 300$  MPa. The meshing portion hit crack of the specimen was made using brick elements. Because the mesh network is more delicate near to the crack, the number of mesh element was 330,520.

In figure 2 is shown a detail of the area around a tip pierced crack where is observed that the stress distribution

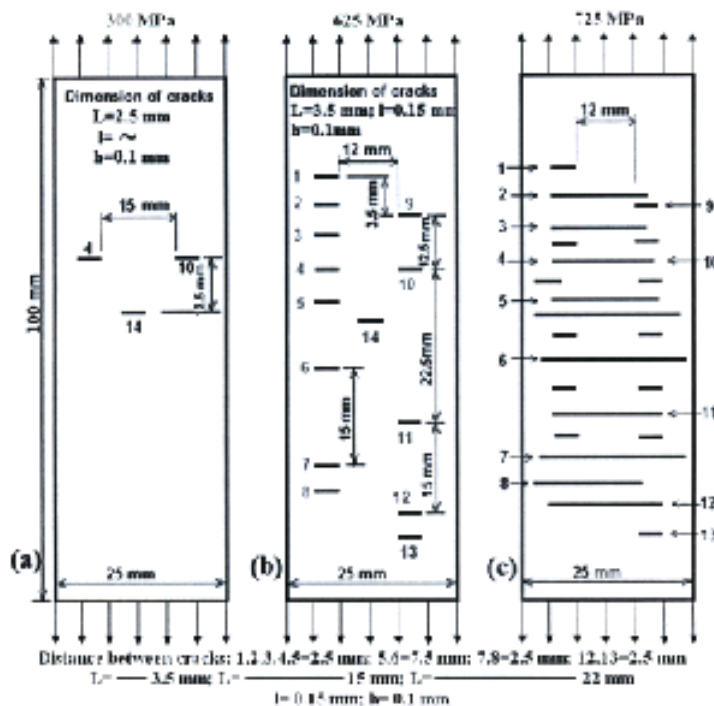


Fig. 1 Schematic representation of transverse cracks in material with increasing of the stress level

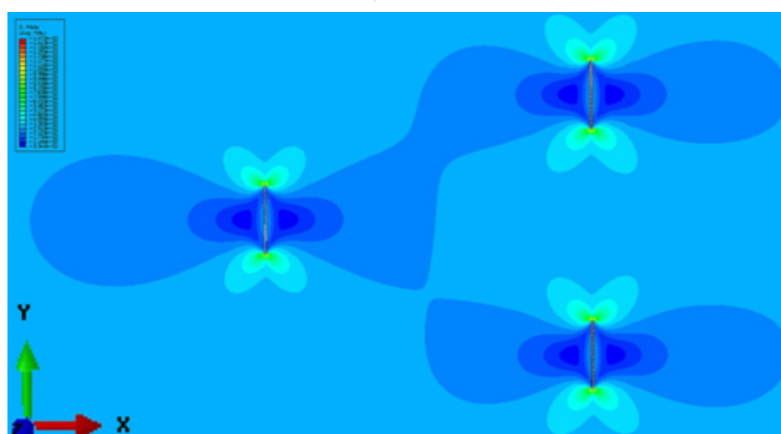


Fig. 2. State of stress (von Mises) around the cracks

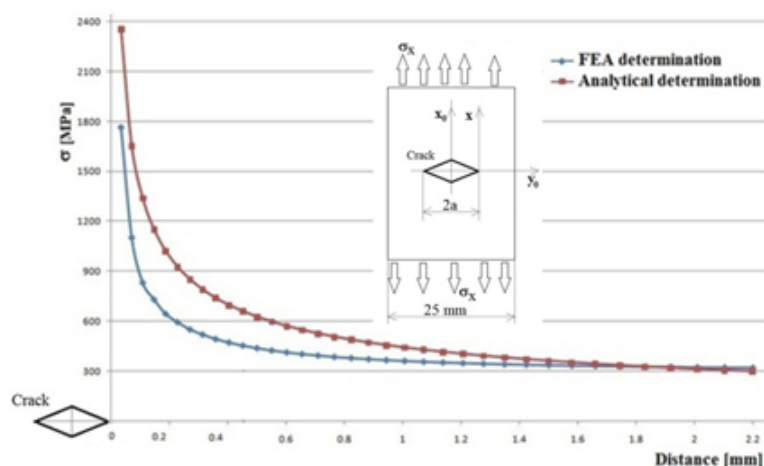


Fig. 3. State of normal stress  $\sigma_x$  at a tip of pierced crack (homogeneous and isotropic material)

at the crack tip is qualitatively similar to that known from Fracture Mechanics [20, 21]. Therefore, the high stresses areas which appear in the vicinity of the cracks are according to von Mises criteria, which establish the area most likely to deform plastically. This area depends on the load, the orientation of the cracks compared to the load and the material characteristics.

For a quantitative verification, in figure 3 was drawn the stress variation  $\sigma_x$  to tip crack. Because, the stress state  $\sigma_x$  in the vicinity of the pierced tip crack of the specimen made of isotropic material, obtained with FEA (blue) and by analytical relations (red) [20, 21] are similar; this represents a validation of the numerical analysis results. Consequently,

FEA can be extended to orthotropic material specimen with pierced and inside cracks. These analyzes will be presented in figure 3.

#### Specimen of homogeneous and orthotropic material

For this material, the stress state in the vicinity of the crack was not possible to compare with data existing in literature. In consequence, for verification, a simulation was performed for a specimen with pierced cracks. The size and location of cracks are identical as in homogeneous and isotropic material (fig. 1a). In this case, the state of stress around cracks (fig. 4), is similar with this known of Fracture Mechanics [20, 21]. However, due to the material



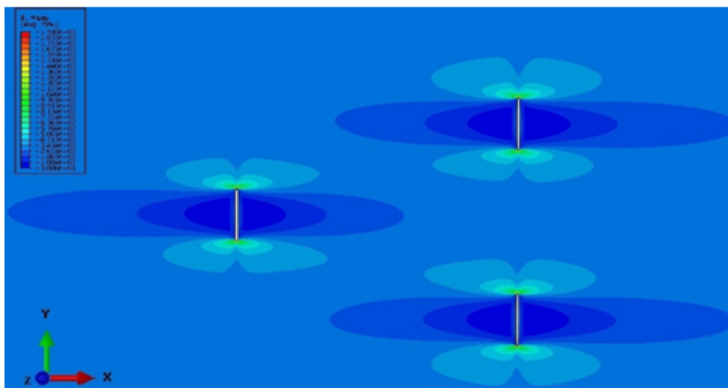


Fig. 4. State of stress (von Mises) around the crack (homogeneous and orthotropic material)

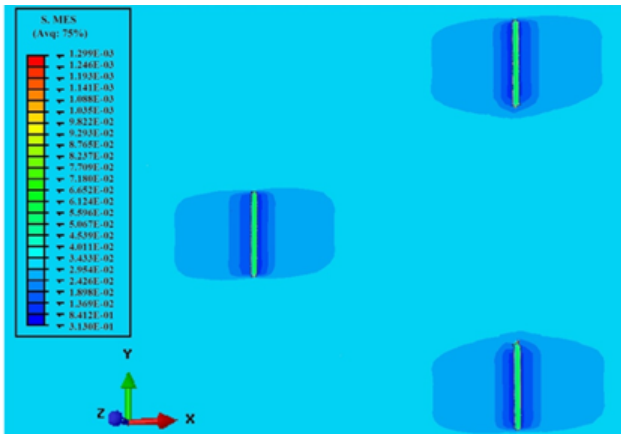


Fig. 5. State of stress (von Mises) around included cracks (homogeneous and orthotropic material)

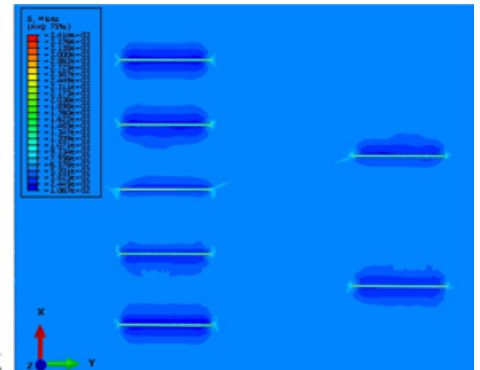
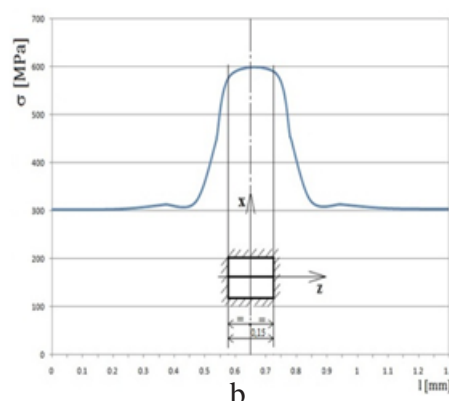
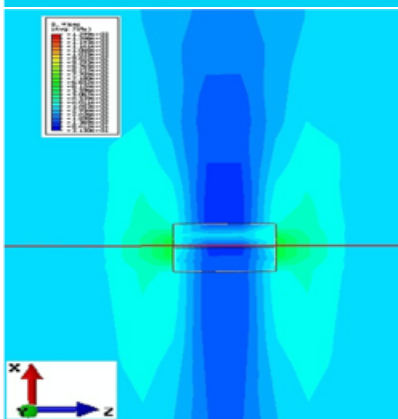


Fig 7 State of stress (von Mises) in specimen around a crack

Fig. 6 State of stress (von Mises) around a crack: a) cross section through the crack (in zOx plan) ; b) stress variation in the Oz axis direction

enforcement, the stresses in the vicinity of the crack do not influence each other as the ones shown in figure 2. Comparing figure 4 for homogeneous and orthotropic material with figure 2 for homogeneous and isotropic material, in the vicinity of the top of the crack a similar stress state appears. This step was necessary in order to check the quality of the results obtained with FEA for cracks in homogeneous and orthotropic material.

### Specimen made of homogeneous and orthotropic material with included cracks

Specimen with included cracks, loaded up to  $\sigma = 300$  MPa  
In specimen were introduced three cracks as it is shown in figure 1a and with dimensions:  $2.5 \times 0.15 \times 0.1$  mm ( $L \times l \times h$ ). Because, from literature it was found experimentally that the first cracks appear to inside of specimen in lamina oriented at  $[90^\circ]$ , in this case the cracks width was taken equal to that of a lamina ( $l = 0.15$  mm). Also, the cracks were positioned in the median plane of the specimen. The meshing portion whit crack of the specimen was made using brick elements and the number was 330,520. Then the specimen was simulated to tensile load up to 300 MPa, figure 5. There it is seen a disturbance

in the stress around the cracks, but these stress have lower values than those in remote areas, where the presence of the cracks do not occur. Also, these cracks are sufficiently distant, so that their neighborhood stresses not influence each other (not *interfere*).

Figure 6 shows a cross section through the crack (in zOx plan). The state of stress (von Mises) around cracks is shows in figure 6a. In figure 6b is presented the variation of von Mises stress on the Oz axis direction (red line of fig. 6a). It is seen that in the middle of crack, the von Mises stress reach a value of 600 MPa, double the nominal stresses  $\sigma_x = 300$  MPa. These high values of stress in the vicinity of crack can cause its propagation.

Specimen with included cracks, loaded up to  $\sigma = 625$  MPa

For the level of stress  $\sigma = 625$  MPa, in the specimen were introduced a more cracks, according to X ray pictures [7] shown in figure 1b. The specimen is mixed meshed using 448,189 finite elements type brick and pyramid, with a denser network mesh near to the cracks. Because the residual stresses are high in specimen edges, the cracks will appear in this area. Also, a higher level of positive residual stresses will cause a higher number of cracks.

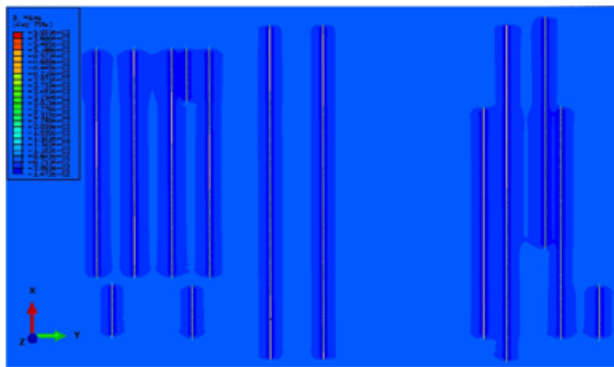


Fig. 8 Von Mises stress distribution in the vicinity of cracks (nominal stress  $\sigma_x = 725$  MPa)

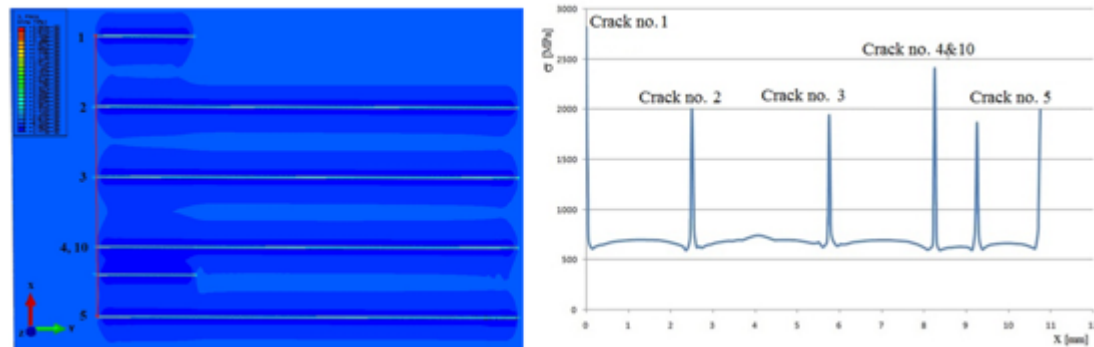


Fig. 9. Variation of von Mises stress at the tip of crack 1÷5 and 10: a) around cracks; b) to tip of cracks (red line direction)

Typically, they are propagated from the edges to the center of the specimen, which can be merged with each other [7].

In figure 7 is presented the variation of von Mises stress of loaded specimen up to nominal stresses  $\sigma_x = 625$  MPa. It is seen that the maximum stress occurs at the tip of cracks and the stresses in the vicinity of the cracks not influencing each other (*not interfere*).

Specimen with included cracks, loaded up to  $\sigma = 725$  MPa

Like is shows in [7], for the 725 MPa value of stress (whit shortly time before the failure of specimen), the cracks are increasing, merged the each other. Also, for this level of load the new cracks appear. For FEA of specimen loaded to nominal stress  $\sigma_x = 725$  MPa, in specimen were introduced the cracks with dimension and number presented in figure 1c. The specimen is mixed meshed using 1,493,821 finite elements, brick and pyramid type.

In figure 8 is presented the variation of von Mises stress of around of cracks. It is seen that the maximum stress occurs, also in this case, at the tip of crack. The stresses in the vicinity of the cracks start to influencing each other, in other words *interfere with each other*. In figure 9 is presented the variation of von Mises stress at the tip of cracks no. 1÷5 and 10 (red line direction). In figure 9b it is seen that the peaks of stress near tip of cracks have values around 2000 MPa, which inevitably will lead to imminent failure of the specimen.

## Conclusions

Using ABAQUS V 6.12 software was performed an analysis whit finite element of specimens with included cracks that occur in the tensile loaded specimens, made of homogeneous and orthotropic material, for three levels of nominal stress: 300 MPa, 625 MPa and 725 MPa.

In the vicinity of included cracks were found double values of von Mises stress in comparison with nominal stress in specimen ( $\sigma = 300$  MPa). For nominal stress  $\sigma = 725$  MPa, the cracks increase both in number and in size, some extending over almost the entire width of the specimen. The stress field adjacent cracks is extends and

the von Mises stresses of tip cracks can exceed 2000 MPa, leading to the imminent failure of the specimen.

Because are not known numerical and experimental results on the state of stress in homogeneous and orthotropic composites materials with included cracks, check the results of the FEA was made by the following methods:

- state of stress in specimen without cracks was compared with known results of Strength of Materials;
- state of stress at the tip of pierced cracks in homogeneous and isotropic material was compared with that calculated by analytical relations of Fracture Mechanics;
- state of stress near the tip of pierced cracks in homogeneous and orthotropic material and isotropic respectively were compared and they have found to be similar.

Considering the above, we can say that the FEA can provide reliable results on the micromechanics of composites with pierced and included cracks if a sufficiently dense and correctly distributed mesh are used and the validation is performed with known models and compared with experimental data or, in their absence, following a logical modeling protocol. It should be mentioned, however, the extreme difficulty of addressing these investigations by other methods (analytical and experimental).

Among the difficulties of method is stated:

- need of a dense network (more fine in the area cracks) with a large number of mesh elements;
- need of manual composition of the network;
- absence of comparison data (experimentally or analytically obtained) for homogeneous and orthotropic material with cracks.

*Acknowledgements: This paper was realized with the support of EURODOC Doctoral Scholarships for research performance at European level project, financed by the European Social Found and Romanian Government. The composite materials have been made in Katholieke University Leuven, MTM Department, Belgium. Tensile tests were performed at Katholieke University Leuven, MTM Department, Belgium and ultrasound test were performed at National*

## References

1. MCCARTNEY, L.N., Theory of stress transfer in a  $0^\circ$ – $90^\circ$ – $0^\circ$  cross-ply laminate containing a parallel array of transverse cracks. *Journal of the Mechanics and Physics of Solids* 40, 1992, p. 27.
2. TRUONG CHIT, VETTORI, M., LOMOV, S. V., VERPOEST, I., Carbon composites based on multiaxial multiply stitched preforms. Part 4, Mechanical properties of composites and damage observation. *Composites, Part A* 3, 2005, p. 1207.
3. EDGREN, F., MATTSSON, D., ASP, L.E., VARNA, J., Formation of damage and its effects on non-crimp fabric reinforced composites loaded in tension. *Composite Science and Technology* 64, 2004, p. 675.
4. LOMOV, S.V., IVANOV, D.S., TRUONG, T.C., VERPOEST, I., Experimental methodology of study of damage initiation and development in textile composites in uniaxial tensile test. *Composites Science and Technology* 68, 2008, p. 2340.
5. OKABE, T., SEKINE, H., NODA, J., NISHIKAWA, M., TAKEDA, N., Characterization of tensile damage and strength in GFRP cross-ply laminates. *Materials Science Engineering A*, 2004, p. 381.
6. BONIFACE, L., SMITH, P.A., BADER, M.G., REZAIFARD, A.H., Transverse ply cracking in cross-ply CFRP laminates–Initiation or propagation controlled. *J of Composite Materials* 31, 1997, p. 1080.
7. GORBATIKH, L., LOMOV, S.V., KLUMP DE BOER, R., Micro-mechanical model for two-step optimization supported by material characterization. *Automated Preform Fabrication by Dry Tow Placement(AUTOW)*, Report DE-20-KUL-WP 3.2-02, 2010.
8. TRUONG, T.C., VETTORI, M., LOMOV, S.V., VERPOEST, I., Carbon composites based on multi-axial multi-ply stitched preforms. Part 4. Mechanical properties of composites and damage observation. *Composites Part A* 36(9), 2005, p. 1207.
9. PARLEVLIET, P.P., BERSEE, H.E.N., BEUKERS, A., Residual stresses in thermoplastic composites—a study of the literature. Part III, Effects of thermal residual stresses. *Composites Part A* 38, 2007, p. 1581.
10. OKABE, T., NISHIKAWA, M., TAKEDA, N., Numerical modeling of progressive damage in fiber reinforced plastic cross-ply laminates. *Composites Science and Technology* 68, 2008, p. 2282.
11. \*\*\* ASTM Standard ASTM D3171-11, Standard Test Methods for Constituent Content of Composite Materials. ASTM International, West Conshohocken, PA, www.astm.org, 2011.
12. \*\*\* ASTM Standard D 3039/D3039M-08, Standard Test Method for Tensile Properties of Polymer Matrix Composite Materials”. ASTM International, West Conshohocken, PA www.astm.org, 2008.
13. KRAUTKRAMER, J., KRAUTKRAMER, H., *Ultrasonic Testing of Materials*”, 4<sup>th</sup> edition. Ed. Springer-Verlag, Berlin, 1990.
14. MARSH, B., The European Classification of Exposure Environmental for Concrete. *Concrete* 34, Nr. 6, 2000.
15. LAWSON, I., DANSO, K.A., ODOI, H.C., ADJEI, C.A., QUASHIE, F.K., MUMUNI, L.I., IBRAHIM, I.S., Non-Destructive Evaluation of Concrete using Ultrasonic Pulse Velocity. *Research Journal of Applied Sciences, Engineering and Technology* 3(6), 2011, p. 499.
16. WROBEL, G., WIERZBICKI, L., Ultrasonic methods in diagnostics of polyethylene. *Archives of Materials Science and Engineering* 28, 2007, p. 413.
17. GRIMBERG, R., SAVIN, A., STEIGMANN, R., BRUMA, A., BARSANESCU, P.D., SALAVASTRU, D.P., Determination of CFRP's mechanical properties using ultrasound methods. V<sup>th</sup> Workshop NDT in Progress, Praga, Czech Republic, 2009, p. 65.
18. \*\*\*, ABAQUS v. 6.11 – User's Manual.
19. TIMOSHENKO, S.P., GOODIER, J.N., *Theory of Elasticity*, 3<sup>rd</sup> Ed. McGraw-Hill, New York, 1970.
20. BROEK, D., *Elementary Engineering Fracture Mechanics*, 4<sup>th</sup> Ed. Kluwer Academic Pub., Dordrecht, 1986.
21. BALKE, A., *Practical Fracture Mechanics in Design*. Marcel Dekker Inc., New York, 1996

Manuscript received: 15.10.2015